Journal of Membrane Science 732 (2025) 124245

Contents lists available at ScienceDirect

Journal of Membrane Science

journal homepage: www.elsevier.com/locate/memsci

GO as gutter layer in superglassy thin film composite membranes for enhanced gas separation

Boya Qiu [a], Ming Yu [b,c], Mustafa Alshurafa [b], Pablo López-Porfiri [a], Maria Perez-Page [a], Andrew B. Foster [b], Peter M. Budd [b], Xiaolei Fan [a,d,*], Patricia Gorgojo [a,e,f,**]

[a] Department of Chemical Engineering, The University of Manchester, Oxford Road, Manchester, M13 9PL, United Kingdom
[b] Department of Chemistry, The University of Manchester, Oxford Road, Manchester, M13 9PL, United Kingdom
[c] Department of Chemical Engineering, The University of Melbourne, Melbourne, VIC, 3010, Australia
[d] Nottingham Ningbo China Beacons of Excellence Research and Innovation Institute, University of Nottingham Ningbo China, 211 Xingguang Road, Ningbo, 315100, China
[e] Instituto de Nanociencia y Materiales de Aragón (INMA) CSIC, Universidad de Zaragoza, Spain
[f] Departamento de Ingeniería Química y Tecnologías del Medio Ambiente, Universidad de Zaragoza, Spain

ARTICLE INFO

Keywords:
Polymer of intrinsic microporosity (PIM)
Gas separation
Thin film composite membranes
Graphene oxide
Gutter layers

ABSTRACT

Polymers with intrinsic microporosity (PIM) have gathered considerable attention over the last two decades for fabricating high-performance membranes for CO_2 separation, owing to their highly permeable and porous structures. Particularly, thin film composite (TFC) membranes with thin active layers (<5 μm) deposited onto more porous substrates are suitable for practical applications as they offer a combination of high permeance and mechanical strength. However, penetration of the active layer into the pores of the substrate leads to additional mass transfer resistance and creates defects and voids, thereby reducing the membrane's permeance and selectivity. Herein, we introduced graphene oxide (GO) as a gutter layer in TFCs made with PIM-1. GO flakes were deposited to cover the substrates partially, thereby reducing polymer penetration while maintaining good structural integrity of the TFCs. We successfully fabricated a series of PIM-1 TFCs by kiss coating, with the thinnest active layer at ~179 nm. These TFCs exhibited an ideal selectivity for CO_2/N_2 of 44.4, and the CO_2 permeance was increased by up to 104 % under optimised conditions. The strategy is generic as well which was validated using carboxylated PIM-1 (cPIM-1).

1. Introduction

Greenhouse gases, especially CO_2, are believed to be responsible for global climate change [1]. Membrane technology has been recognised as a promising method for CO_2 separation in carbon capture, with the advantages of low capital and operating costs, ease of operation, and minimal energy consumption. However, the energy efficiency of an industrial-scale membrane separation system is largely dependent on the selectivity and permeability of the membranes [2]. Among various polymeric membranes, those made of superglassy polymers with semi-rigid microporous structures [3,4] feature both ultra-micropores (<7 Å) and micropores (7–20 Å). The ultra-micropores provide molecular sieving function for improving molecule-pair selectivity, while the micropores facilitate fast permeation [5]. Consequently, the superglassy polymer membranes demonstrate a superior combination of high permeability and reasonable selectivity compared to many traditional polymer membranes, defining the most recent upper bounds for CO_2 separation [6,7]. Besides, superglassy polymer membranes offer advantages such as ease of membrane fabrication and higher membrane flexibility than the membranes composed of rigid crystalline microporous materials such as carbon molecule sieves [8,9], metal-organic frameworks (MOFs) [10,11], and covalent organic frameworks (COFs) [12].

Among superglassy polymer materials, polymers of intrinsic microporosity (PIMs), composed of contorted ladder polymer chains that pack inefficiently in the solid state, have relatively large micropores. Hence, PIMs exhibit higher permeability (up to 50,000 barrer for CO_2 [7]) than most other polymers, while maintaining reasonably good selectivity [4].

* Corresponding author. Department of Chemical Engineering, The University of Manchester, Oxford Road, Manchester, M13 9PL, United Kingdom.
** Corresponding author. Departmento de Ingeniería Química y Tecnologías del Medio Ambiente, Universidad de Zaragoza, Spain.
E-mail addresses: xiaolei.fan@manchester.ac.uk (X. Fan), pgorgojo@unizar.es (P. Gorgojo).

https://doi.org/10.1016/j.memsci.2025.124245
Received 24 March 2025; Received in revised form 13 May 2025; Accepted 19 May 2025
Available online 19 May 2025

To date, most research on PIMs has focused on self-standing membranes with thicknesses exceeding 20 μm. Yet, thin film composite (TFC) membranes (consisting of a thin active layer, typically <5 μm, and a robust porous membrane substrate) are used for practical applications because they offer high gas permeance with less amount of polymer materials and have good mechanical strength. Taking the prototype PIM-1 as an example, several strategies have been adopted for fabricating defect-free TFCs with low active layer thickness, such as dip coating/kiss coating [13–22], spin coating [23–27], bar coating [28], and electrospraying [29]. Nevertheless, excessive polymer penetration into the porous substrate remains a common issue in these methods. Indeed, a certain degree of penetration is necessary for anchoring the active layer to the membrane substrate, but excessive penetration leads to additional mass transfer resistance, thus decreasing membrane permeance. In some cases, it also causes inhomogeneity in the active layer, resulting in significant defects/voids formation and thus reducing membrane selectivity. In particular, casting solutions of superglassy polymers are less viscous than those of conventional rubbery polymers such as polydimethylsiloxane (PDMS), and thus they experience penetration to a greater extent.

To mitigate polymer penetration, the membrane substrate is preferably engineered with a skin layer having smaller pores and more uniform distribution, while maintaining the pristine bulk porosity for low mass transfer resistance. Among various substrates such as anodic aluminium oxide (AAO) [23–25], polyvinylidene difluoride (PVDF) [30–32], MFFK-1 [15], and polysulfone (PSF) [28], polymeric substrates based on polyacrylonitrile (PAN) are widely used for the preparation of PIM-1 TFC membranes due to their flexibility and well-optimised surface, with pores ranging from 10 to 50 nm [13,14,16,18–22,26,29,33]. However, severe penetration of PIM-1 into PAN was still noticed [21]. Notably, most commercial PAN substrates were originally developed for ultrafiltration applications and were not specifically optimised for use as supports in gas separation membranes. Consequently, the development and optimisation of PAN substrates tailored for gas separation remains a critical challenge and require further investigation.

Alternatively, enhancing the separation performance of TFC membranes using existing commercial substrates might be a more practical approach, which could achieve meaningful performance improvements within current material constraints, as well as being readily adapted to future substrate innovations. Focusing on this approach, we have explored a solvent pre-filling method, in which the pores of the substrate are pre-wetted with solvents such as water, ethanol, methanol, or chloroform prior to polymer coating [32,34]. This technique has been shown to improve selectivity by up to ~40 % in pervaporation [32]. However, it is less suitable for gas separation, as interactions between the solvent and polymer can induce subtle structural variations that may lead to separation failure. Another approach involves introducing a polymeric gutter layer, such as poly(1-trimethylsilyl-1-propyne) (PTMSP) [15] and PDMS [26–28], which can effectively suppress PIM-1 penetration into the porous substrate. Nevertheless, these materials often necessitate relatively thick coatings (typically 210 nm to 2.5 μm), which add considerable mass transfer resistance, thus compromising overall membrane performance. Hence, an optimal strategy to prevent polymer penetration without significantly increasing mass transfer resistance remains a key objective for advancing high-performance TFC membrane design.

In this work, we report the use of graphene oxide (GO) as a gutter layer on porous PAN substrates to fabricate TFC membranes based on the superglassy polymer of intrinsic microporosity, PIM-1. GO, a two-dimensional material with a lateral size exceeding 500 nm, is impermeable to liquids and gases [35], and can be feasibly retained on porous substrates through vacuum filtration [36,37]. This technique also enables precise control over GO loading and layer thickness, offering flexibility in balancing polymer penetration and mass transfer resistance. By tuning GO loading, we optimised the deposition of impermeable GO flakes to achieve partial surface coverage. This design aimed to effectively reduced PIM-1 penetration while intentionally retaining some uncovered pores, thereby preserving high gas permeance and ensuring proper integration between the selective layer and the substrate. The reduced penetration of PIM-1 by the GO gutter layer was validated according to the morphology analysis of the TFC membranes. Additionally, the gas permeance and ideal selectivity of CO_2/N_2 were measured for relevant TFC membranes to assess the effectiveness of the developed strategy. Importantly, this approach is generic, as demonstrated by using carboxylated PIM-1 (cPIM-1).

2. Methods

2.1. Materials and chemicals

PIM-1 (MY-B03, M_n = 57,500 g/mol, M_w = 166,900 g/mol, and polydispersity M_w/M_n = 2.9) was obtained through the procedure shown in Supplementary Information. cPIM-1 was synthesised through the procedure reported by Rodriguez et al. [38]. Two batches of polyacrylonitrile (PAN) substrate with reference PAN350 (thickness 165 μm) were purchased from Sepro Membranes, USA. Slide-A-Lyzer G2 Dialysis Cassette (2K MWCO) was obtained from Thermo Fisher Scientific. Chemicals, including natural graphite, H_2SO_4, $K_2S_2O_8$, P_2O_5, $KMnO_4$, H_2O_2, HCl, and chloroform, were used without further purification.

2.2. Membrane fabrication

The GO was deposited on the PAN substrate by vacuum filtration. A certain amount of GO dispersion was diluted with DI water (500 mL) to prepare a GO suspension with a concentration of <0.5 mg/L. After that, the suspension was placed in a sonication bath (Elmasonic P70H, Germany) for 20 min at room temperature. Meanwhile, the PAN substrate was rinsed with DI water and placed on the vacuum filtration set-up, where an active filtration area of 36.3 cm^2 was available for GO deposition. GO dispersions of different concentrations were filtered through the PAN substrate at 0.1 MPa and the prepared GO/PAN membranes were dried in a vacuum oven overnight at room temperature. GO/PAN with different loadings of GO was prepared, including 1, 3, and 5 mg m^{-2}. The loading of GO was calculated by Equation (1):

$$\eta = \frac{c \times V}{S} \tag{1}$$

where c and V are the concentration (mg mL^{-1}) and volume of GO (mL) in aqueous solution, respectively, S is the active filtration area (m^2) of the vacuum filtration. The prepared membranes were stored at room temperature before use.

PIM-1 coating solutions with concentrations in the range 0.5–2.5 w/v%, were used to prepare TFN membranes via kiss coating, onto PAN and GO-coated PAN substrates. The coating procedure is described in Supplementary Information.

2.3. Characterisation

GO was characterised by X-ray powder diffraction (XRD), attenuated total reflectance Fourier transform infrared spectroscopy (ATR-FTIR), atomic force microscopy (AFM), and transmission electron microscopy (TEM) to confirm its chemical structure. Before characterization of XRD and FTIR, a certain amount of GO was dried from its dispersion in a vacuum oven overnight at room temperature. The GO/PAN substrates and PIM-1 TFC were characterised by scanning electron microscopy (SEM) and AFM. Details of the characterisation procedure is described in Supporting Information.

2.4. Gas separation

Details of the gas separation procedure and calculations can be found

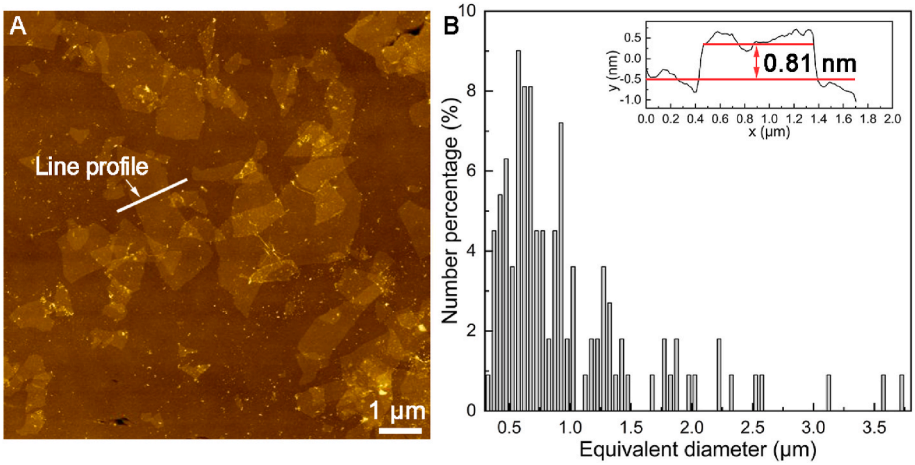

Fig. 1. Morphological characteristics of GO flakes (A) AFM height image of GO flakes; (B) size distribution of GO flakes (inset: height profile of GO flakes).

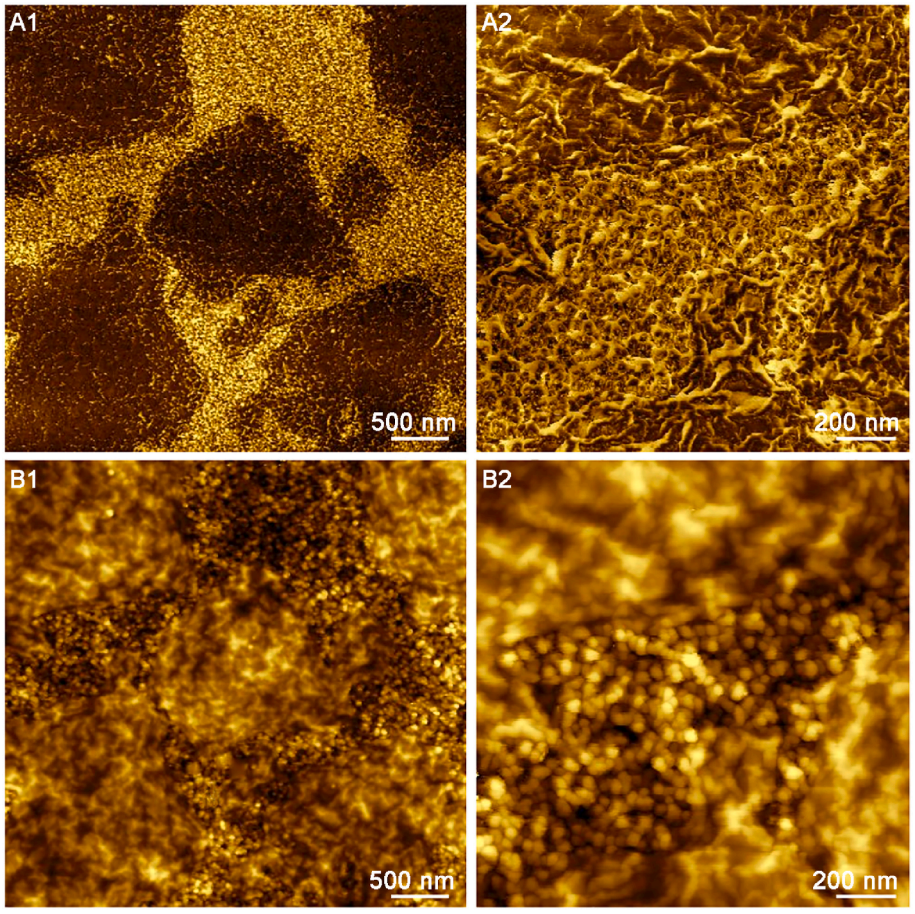

Fig. 2. Surface topology of GO/PAN (A) AFM height images; (B) AFM phase images (loading of GO at 1 mg m^{-2}).

in the Supporting Information.

3. Results and discussion

3.1. Optimisation of the GO gutter layer

GO flakes were synthesised using a modified Hummer's method [39]. The physicochemical properties of the prepared GO were characterised by FTIR, XRD (Fig. S1) and AFM (Fig. 1). The lateral size and thickness of the GO flakes were estimated based on the AFM height image (Fig. 1A).

The thickness of the GO flakes was measured at 0.81 nm, as shown in the inset of Fig. 1B, which aligns the reported thickness of single-layer graphene oxide [40]. For lateral dimensions, statistical analysis of over 100 flakes revealed a relatively broad size distribution, with the majority of flakes ranging between 0.4 and 1 μm (Fig. 1B). These dimensions are 1–2 orders of magnitude larger than the average pore size of the PAN substrate (~20 nm), thereby ensuring effective retention of GO flakes on the substrate surface during vacuum filtration.

Achieving optimum GO coverage on the PAN substrate is crucial for

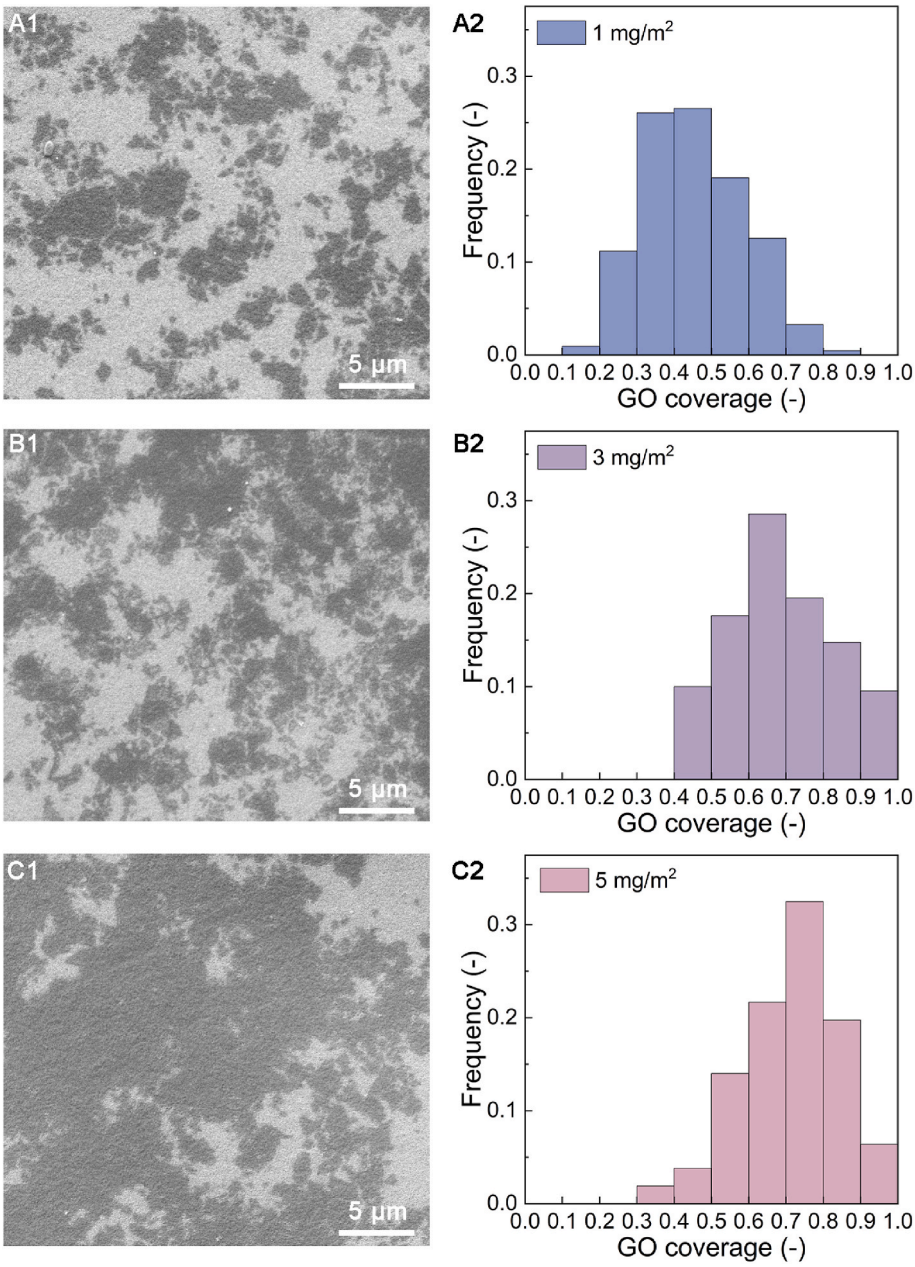

Fig. 3. Representative SEM images of GO/PAN with different loadings of GO: (A) 1 mg m^{-2}, (B) 3 mg m^{-2}, and (C) 5 mg m^{-2}, and statistical coverage.

developing a high-performance TFC. In this study, GO flakes were deposited onto PAN via vacuum filtration of a 500 mL aqueous GO suspension. By adjusting the GO concentration in the suspension (0.007–0.036 mg/L), loadings of 1–5 mg m^{-2} were obtained, resulting in different degrees of surface coverage on the PAN substrates. AFM phase images of the GO/PAN surface confirmed the presence of flakes (Fig. 2A). In addition, AFM height-mode roughness analysis (Fig. 2B) revealed that GO deposition led to a smoother surface (roughness of 4.2 ± 0.6 nm) compared to the pristine PAN substrate (roughness of 6.2 ± 0.4 nm).

GO deposition onto PAN from suspensions of different concentration was also assessed by SEM. Based on analysis of over 200 SEM images of the membrane surface (Fig. 3A1, 3B1, and 3C1), it was observed that GO coverage increased with higher GO concentrations in suspensions (Fig. 3A2, 3B2, 3C2 and Figure S2). At the lowest loading of 1 mg m^{-2}, most GO flakes appeared as isolated "islands" with lateral dimensions ranging from 0.1 to 0.8 μm, with only a few clusters coalescing into lateral sizes of approximately 3 μm (Fig. 3A2). In contrast, at higher loading of 5 mg m^{-2}, flakes overlapped and formed large "continents" with lateral dimensions exceeding 10 μm (Fig. 3C2). Given that the GO interlayer between the active layer and the PAN support alters the mass transfer pathway by promoting lateral gas transport, a lower GO loading with isolated flakes is expected to impose less additional mass transfer resistance due to the shorter lateral diffusion path. Additionally, GO flakes tend to deposit preferentially in regions with larger surface pores or defects, where local water flow rates during vacuum filtration are higher. This explains the non-uniform GO distribution observed in SEM images, which is likely a reflection of the inherent non-uniformity in the PAN substrate. As a result, GO deposition may serve a selective "healing" function, sealing larger pores and surface defects that would otherwise facilitate PIM-1 penetration, which can lead to defect formation in the TFC selective layer during coating.

CO_2 permeance was evaluated for PAN and GO/PAN substrates with GO loadings of 1, 3, and 5 mg m^{-2}. All membrane substrates exhibited

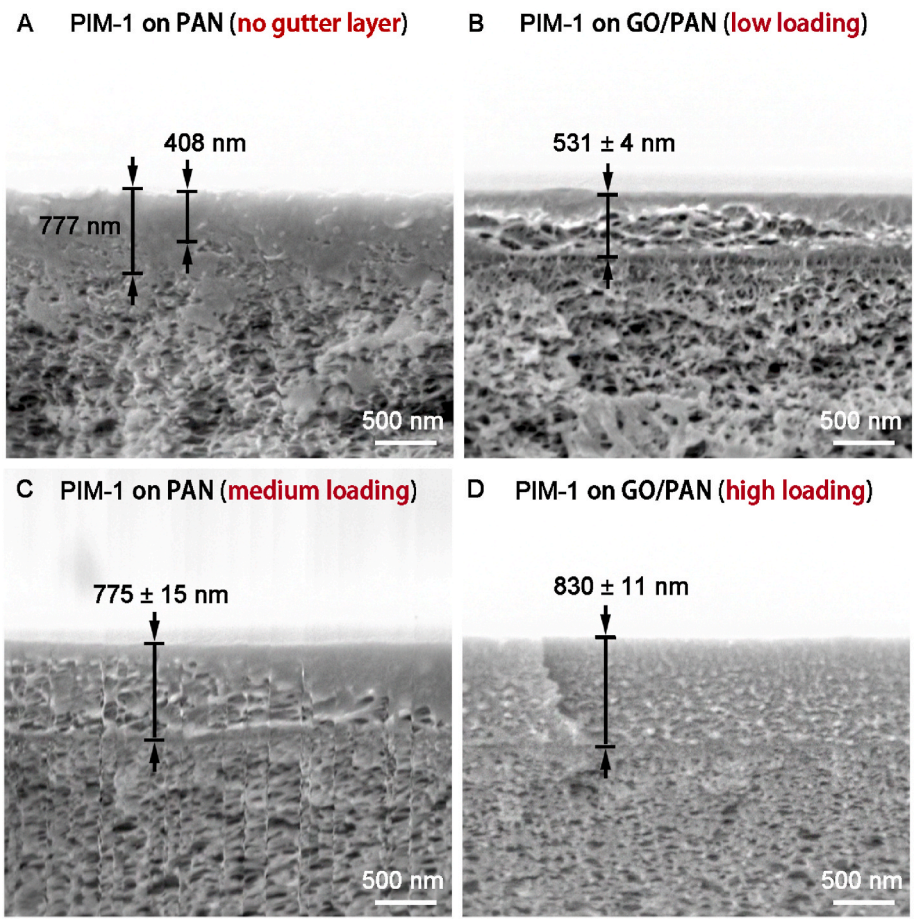

Fig. 4. Cross-sectional SEM images of PIM-1 TFC membranes on PAN (A) and GO/PAN with GO loadings of (B) 1 mg m^{-2}, (C) 3 mg m^{-2}, and (D) 5 mg m^{-2} (coated by PIM-1 solution at 2.0 w/v%).

high CO_2 permeance values exceeding 70,000 GPU, indicating that a significant fraction of the PAN surface remained uncoated and exposed following GO deposition. These uncovered regions retain their open pore structure, which facilitates convective gas flow with minimal resistance.

3.2. Coating of PIM-1 onto GO/PAN

PIM-1 TFC membranes were fabricated by kiss coating PIM-1 solutions at a range of concentrations (0.5–2.5 w/v%) onto GO-coated and non-coated PAN substrates. It is assumed that GO distribution remains intact during PIM-1 coating. This assumption is supported by the inherently high surface free energy of GO, which promotes the flakes to strongly adhere to underlying surfaces to minimise interfacial energy. In addition, previous studies have demonstrated that ultrathin GO layers deposited on various substrates including PAN [37,41,42] exhibit high stability even under harsh conditions such as water flushing.

The thickness of the supported PIM-1 layers was measured on cross-sectional SEM images of the TFCs, as shown in Fig. 4. For the control membrane fabricated on pristine PAN using a 2 w/v% PIM-1 solution without a gutter layer (Fig. 4A), significant penetration of PIM-1 into the PAN substrate was observed. This resulted in considerable variations in measured thickness values (408–777 nm). It is deduced that 408 nm reflects the actual thickness of the PIM-1 active layer, whereas 777 nm includes regions where PIM-1 penetrated and completely filled substrate pores.

In contrast, for membranes incorporating GO gutter layers at 1 mg m^{-2} (Fig. 4B), no visible PIM-1 penetration into the PAN substrate was observed. The PIM-1 layer was clearly distinguishable with a uniform thickness of 531 ± 4 nm, which is approximately 30 % lower than the effective thickness on bare PAN, confirming the effectiveness of GO in preventing polymer penetration.

As the GO loading increased (Fig. 4C and D), a distinct interface between the PIM-1 layer and the PAN substrate remained visible, suggesting suppression of PIM-1 penetration. However, the thickness of the PIM-1 layer increased with higher GO loadings. This may be attributed to the high affinity between the PIM-1 solution and GO flakes, which can influence the dynamic meniscus curvature during coating. Additionally, the reduced polymer penetration at higher GO loadings likely results in greater retention of PIM-1 at the surface, thereby forming a thicker selective layer.

Based on these findings, a GO loading of 1 mg m^{-2} was selected as optimal and used for subsequent TFC fabrication with PIM-1 solutions at different concentrations (0.5, 1.5, and 2.5 w/v%). Cross-sectional SEM images of the resulting membranes are shown in Fig. S3. All TFCs displayed a well-defined interface between the PIM-1 layer and the substrate, confirming the effectiveness of using GO as a gutter layer to prevent PIM-1 penetration. Furthermore, the thickness of the selective layer increased with the concentration of the PIM-1 solution, consistent with the higher viscosity and reduced flowability of more concentrated solutions. Specifically, membrane thickness ranged from 179 ± 16 nm to 745 ± 10 nm for coating solutions of 0.5 and 2.5 w/v%, respectively.

3.3. Gas separation performance

The separation performance of relevant TFCs was assessed by single-component gas permeation tests (using CO_2 and N_2), from which permeance and ideal selectivity were calculated. All TFC membranes

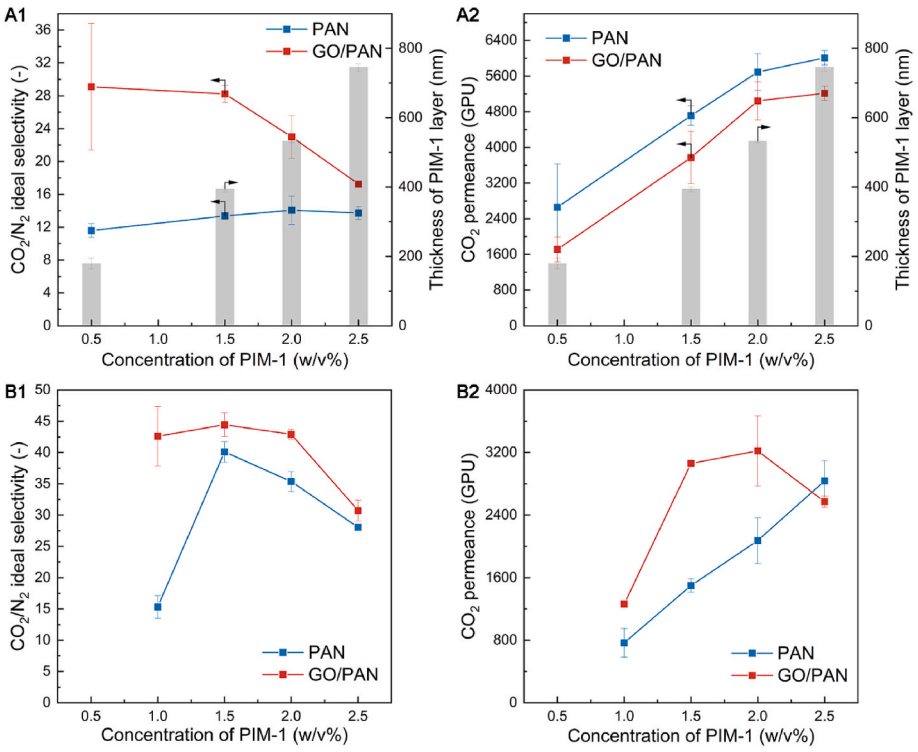

Fig. 5. CO_2/N_2 ideal selectivity and CO_2 permeance of TFC membranes coated with PIM-1 solutions of different concentrations (A) PIM-1 TFC coated on PAN#1 and (B) PIM-1 TFC on PAN#2 (GO loading of GO/PAN at 1 mg m^{-2}; permeance and selectivity are calculated based on the average of at least three measurements; grey column in A1 and A2 indicate thickness of PIM-1 layer on GO/PAN).

demonstrated good mechanical strength and showed no observable delamination during handling or testing. This structural integrity could be attributed to the strong interfacial interactions between GO and PIM-1 [19,43,44], high adherence of GO flakes on PAN substrates [36,45], and partial PIM-1 penetration into the substrate.

As shown in Fig. 5A1 and 5A2, the control membrane, coated with a 2.5 w/v% PIM-1 solution on bare PAN, exhibited a CO_2 permeance of 6007 GPU and a CO_2/N_2 ideal selectivity of 15.2. Generally, thinner membranes are expected to exhibit higher permeance due to shorter gas diffusion paths. However, in this study, thinner membranes fabricated by lower-concentration PIM-1 solutions showed lower permeance than their thicker counterparts. For instance, reducing the PIM-1 concentration from 2.5 to 0.5 w/v% led to a 56 % decrease in CO_2 permeance, to 2659 GPU (Fig. 5A1). This also indicates the lower permeability (permeance × thickness) of PIM-1 in thinner layers.

A similar phenomenon was previously reported by Tiwari et al. [46], where a thin PIM-1 layer (~265 nm) showed a permeability an order of magnitude lower than that of thick films (~30 μm). This reduction is primarily attributed to polymer rigidification near the substrate interface. Strong interactions between PIM-1 and the PAN substrate restrict polymer chain mobility, limiting their ability to expand pore structures transiently and thereby reducing gas transport. Since thinner films have a greater proportion of polymer chains in contact with the substrate, they experience more pronounced rigidification and consequently lower permeability.

Moreover, polymer densification and physical aging may also contribute to reduced gas transport in thin membranes. Gorgojo. et al. [47], reported that ultrathin (~35 nm) PIM-1 membranes exhibited higher stiffness (higher Young's modulus) than thicker membranes (~660 nm) due to polymer densification, which led to ~80 % lower heptane permeability in organic solvent nanofiltration. Besides, physical aging was also reported to be faster in thinner membranes, which could accelerate polymer densification [48]. However, given that all membranes in this study were tested after one-day aging, the impact of aging is expected to be minimal.

Interfacial rigidification often enhances gas selectivity due to tighter pore structures and better molecular sieving, and multiple literature reported that TFC membranes exhibited higher selectivity than their corresponding thick free-standing membranes [13,49,50]. However, this was not the case in the bare PAN-supported membranes. The CO_2/N_2 ideal selectivity of TFCs prepared with a 0.5–2.5 w/v% PIM-1 solution was at 11–14 (Fig. 5A1). Based on statistical analyses of PIM-1 membranes reported from 2005 to 2024, the typical CO_2/N_2 selectivity of free-standing PIM-1 (>20 μm) is ~18 [48]. This suggests that defects in TFCs, especially in thinner selective layers, may offset any gains from rigidification.

In contrast, TFCs fabricated on GO/PAN substrates (GO loading = 1 mg m^{-2}) demonstrated significantly higher selectivity compared to those on bare PAN (Fig. 5A1). The improvement was most pronounced for the TFCs coated using 0.5 w/v% PIM-1 solution, where the ideal CO_2/N_2 selectivity doubled to 29.1. Notably, membranes prepared with 0.5–1.5 w/v% PIM-1 solutions on GO/PAN exceeded the selectivity of free-standing PIM-1 membranes, demonstrating superior performance (>28). This improvement is attributed to the combined effects of interfacial rigidification and a substantial reduction in nano-voids and coating-induced defects when GO is used as a gutter layer. Furthermore, higher selectivity was observed in TFCs prepared from lower-concentration PIM-1 solutions, which can be explained by a higher degree of rigidification in thinner films. Since such rigidification effect induced by substrate surface is confined to polymer chains in close proximity, a greater proportion of the active layer becomes rigidified as layer thickness decreases.

Regarding gas permeance, the addition of the GO gutter layer caused a reduction in CO_2 permeance by 11.3–35.6 %. This could also be attributed to i) elimination of defects, which would otherwise facilitate the rapid transport of both CO_2 and N_2 gases, ii) interfacial rigidification, and iii) a slightly increased effective diffusion path, as the impermeable GO flakes promote lateral gas transport across the membrane

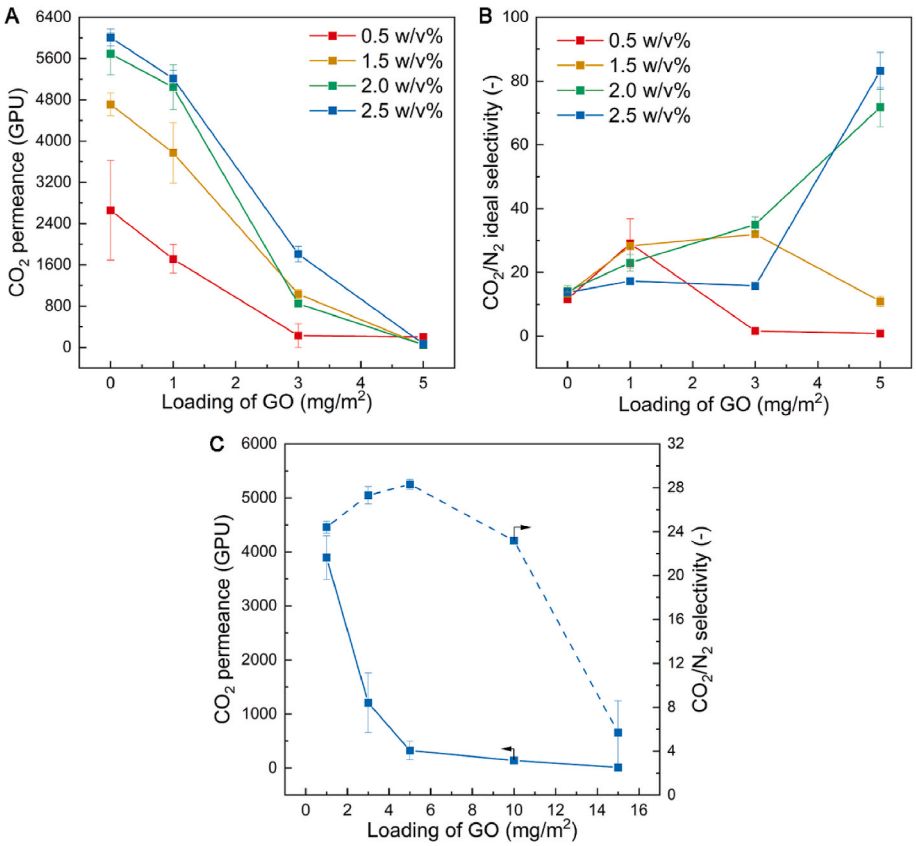

Fig. 6. Effect of GO loading on the permeance and selectivity of PIM-1/GO/PAN (A–B: CO_2 permeance and CO_2/N_2 ideal selectivity of PIM-1/GO/PAN#1 measured by single gas permeance; C: mixed gas separation performance of PIM-1/GO/PAN#2 in separating CO_2/N_2 (1:1) mixture (coated by PIM-1 solution of 2.5 w/v%)). (Permeance and selectivity are calculated based on the average of at least three measurements).

surface. Nevertheless, the impact of lateral transport resistance is expected to be minimal at a GO loading of 1 mg m^{-2}, given the relatively dispersed distribution and small size of the GO flakes.

As the separation performance of PIM-1 TFCs is highly sensitive to the surface morphology and porosity property of the substrate, the PIM-1 TFCs were also prepared on an additional batch of PAN substrates (named PAN#2, the first batch was named PAN#1 for differentiation). While PAN#1 and PAN#2 posessed same performance in ultrafiltration and shared similar surface pore sizes (<40 nm) and porosity (Figure S5A), their cross-sectional structures differed significantly (Figure S5B). Specifically, PAN#1 featured a highly porous inner structure with large channels (up to 450 nm). In contrast, PAN#2 exhibited a skin layer with narrow channels (<100 nm).

TFCs fabricated on PAN#2 without a gutter layer (Fig. 5B) demonstrated higher CO_2/N_2 selectivity (up to 40.1 at 1.5 w/v% PIM-1) and lower CO_2 permeance (700–2800 GPU) than those prepared on PAN#1. This is likely due to narrower pores of PAN#2, which are more easily to be filled by penetrated PIM-1, with less defect formation while increasing mass transfer resistance. Being less compromised by defects, PIM-1 TFC membranes could obtain higher selectivity than the corrosponding thick free-standing membranes, like the findings reported previously [13,49,50]. Similar to TFC on GO/PAN, higher selectivity was also observed in TFCs prepared from lower-concentration PIM-1 solutions due to the higher degree of rigidification in thinner films.

However, when the concentration of the PIM-1 solution was reduced to 1.0 w/v%, excessive penetration into the substrate pores led to defect formation, evidenced by a notable decline in selectivity to 15.3. Notably, introducing a GO gutter layer (1 mg m^{-2}) at this same coating concentration significantly improved gas selectivity to 42.6, confirming the effectiveness of GO in preventing polymer penetration. Similar enhancements in CO_2/N_2 selectivity were observed for TFCs fabricated at other PIM-1 concentrations (1.5, 2.0, and 2.5 w/v%), further demonstrating the ability of GO to suppress defect formation associated with polymer penetration into the porous substrate.

Interestingly, the TFC coated with 1.5 w/v% PIM-1 on GO/PAN#2 exhibited a 104 % increase in CO_2 permeance compared to its counterpart on bare PAN#2 (Fig. 5B2). This enhancement highlights that suppressing polymer penetration shortens gas diffusion path and reduces overall mass transfer resistance. These findings suggest the GO gutter layer imposing insignificant resistance under the optimised condition (GO loading = 1 mg m^{-2}).

An exception was observed in the 2.5 w/v% PIM-1 membrane, where the GO-guttered TFC displayed slightly lower permeance than its non-GO-guttered counterpart. This observation implies that polymer penetration is already sufficiently suppressed at higher polymer concentrations on narrow-pore substrates such as PAN#2. Under such conditions, the slightly increased resistance introduced by the GO layer becomes observable.

Based on these findings, we can conclude that the best-performing membrane without a GO gutter layer in terms of selectivity is the one with 2.5 w/v% PIM-1 on PAN#2. For this membrane, adding GO does not make a significant difference, in terms of both, selectivity and permeance. Furthermore, to improve gas permeance in TFCs prepared onto the substrate with smaller pores, lower PIM-1 concentrations and GO gutter layers should be used in combination, leading also to slightly improved selectivity. If higher gas permeance is sought after, substrates with bigger pores are needed, but in combination with GO gutter layers to achieve a reasonably good selectivity.

To further examine the influence of GO loading, membranes with GO loadings of 1–5 mg m^{-2} were fabricated (on GO/PAN#1) and evaluated (Fig. 6A and B). Increasing the GO loading significantly reduced CO_2 permeance, from 2000 to 6000 GPU (at 1 mg m^{-2}) to <200 GPU (at 5

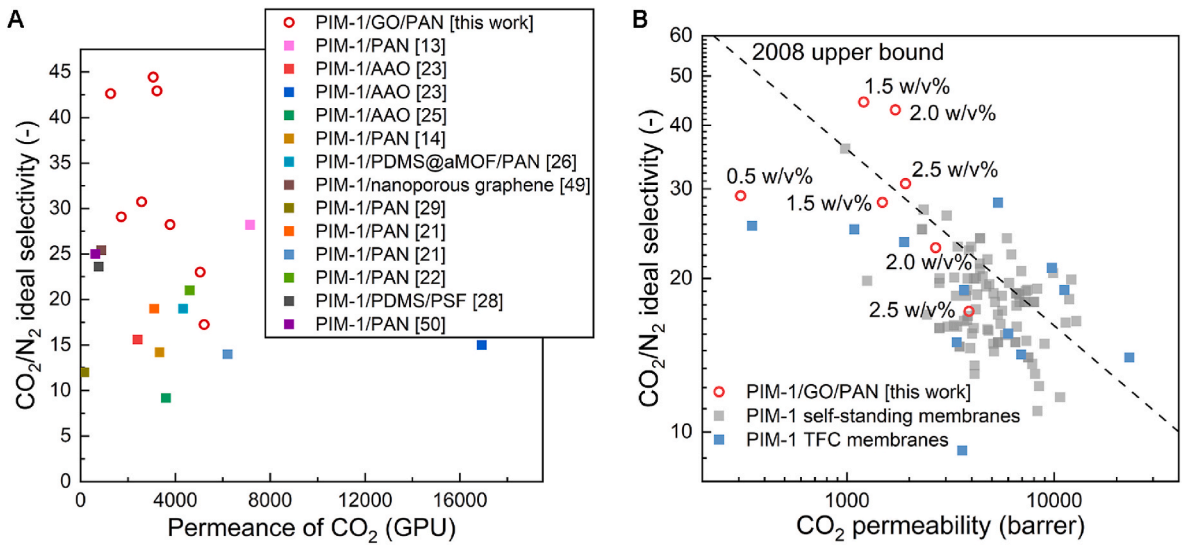

Fig. 7. CO_2 ideal selectivity vs. permeance of the state-of-the-art PIM-1 TFCs on different substrates (A) (plotted data for comparison has been taken from the recent literature [13,14,21–23,25,26,28,29,49,50]); CO_2/N_2 ideal selectivity vs. CO_2 permeability of PIM-1 TFC and free-standing membranes (B) (GO loading of GO/PAN at 1 mg m^{-2}, PIM-1/GO/PAN coated by PIM-1 solution of 0.5–2.5 w/v%).

mg m^{-2}), due to enhanced mass transfer resistance. Since GO is impermeable to both CO_2 and N_2, it blocks direct through-pore pathways and forces gas molecules to traverse longer lateral diffusion paths. At low GO loading (1 mg m^{-2}), this effect is minimal due to the dispersed and isolated nature of the small flakes. However, at higher loadings, GO flakes merge into laminated "continents" exceeding 20 μm in lateral size, which is over 20 times the thickness of the PIM-1 layer (0.2–0.8 μm), drastically increasing diffusion path length and resistance.

At high GO loading (e.g., 5 mg m^{-2}), an additional diffusion pathway may arise, whereby gas molecules travel through the interlayer spacings of the stacked GO flakes. However, this route introduces further resistance due to narrow and tortuous channels. For instance, Kim et al. [51] reported that a 3 nm-thick GO laminate composed of 250 nm flakes exhibited only ~100 GPU CO_2 permeance and a CO_2/N_2 selectivity of ~10.

Conversley, our PIM-1 TFCs fabricated on GO/PAN substrates at 5 mg m^{-2} GO loading achieved substantially higher CO_2/N_2 selectivities of 71.8 and 83.2 with 2.0 and 2.5 w/v% PIM-1, respectively (Fig. 6B). This result suggests that the dominant gas transport pathway in these membranes is not through the *d*-spacing in stacked GO, but rather laterally through the rigidified PIM-1 selective layer, followed by transport into the uncovered PAN pores. This path involves an increased diffusion distance (up to ~10 μm, thus low permeance of <100 GPU), but benefits from enhanced molecular sieving due to polymer chain rigidification at the GO interface.

For the TFCs with thinner active layers (coated with 0.5 and 1.5 w/v % PIM-1 solutions), excessive GO loadings (3 or 5 mg m^{-2}) resulted in decreased selectivity. This reduction may be attributed to defects caused by poor attachment of the PIM-1 layer to the substrate, due to insufficient penetration, a problem that is more severe for TFCs with thinner active layers. Therefore, a moderate degree of penetration is necessary to ensure good interfacial integrity, particularly for ultrathin active layers.

For the PIM-1 TFCs with a relatively thick active layer (coated with 2.5 w/v% PIM-1 solution) on GO/PAN#2, we further investigated their separation performance for CO_2/N_2 (1:1) mixture (Fig. 6C). Similar to results from single-gas permeation tests, as the GO loading increased from 1 to 5 mg m^{-2}, the CO_2/N_2 selectivity of PIM-1 TFC increased from 24.4 to 27.3, whilst the permeance of CO_2 decreased from 3896 GPU to 325 GPU.

Additionally, substrates with excessive GO loading (to 10 and 15 mg m^{-2}) were prepared as well to demonstrate its effect on membrane performance. These membranes exhibited a significant decline in both selectivity and permeance. Such performance degradation is consistent with the trends observed for PIM-1 TFCs coated with more diluted PIM-1 solutions (0.5 and 1.5 w/v%) on PAN#1. These findings indicate that although TFCs composed of thicker active layers have relatively better structural integrity, they suffer from poor attachment to the substrate when polymer penetration is too low. Furthermore, at higher GO loadings, the substrate surface becomes almost entirely covered by GO flakes, forcing gas molecules to diffuse through the narrow *d*-spacing between GO laminates, which reduces both permeance and selectivity. As a result, membranes prepared with 15 mg m^{-2} GO exhibited dramatically reduced CO_2 permeance and selectivity, down to 11 GPU and 6.7, respectively.

Based on the results and previous discussion, the optimum GO loading is 1 mg m^{-2}. The separation performance of the PIM-1 TFCs prepared with 1 mg m^{-2} of GO as the gutter layer was compared with state-of-the-art PIM-1 TFCs fabricated on various substrates including AAO, PAN, and PSF, as well as substrates with a gutter layer, such as PDMS (Fig. 7A and Table S1). The GO/PAN-based TFCs developed in this study outperformed previously reported PIM-1 TFCs in terms of CO_2/N_2 selectivity, while maintaining relatively high CO_2 permeance.

To further assess the transport properties of the selective PIM-1 layer, the permeability of the PIM-1 layer was calculated based on the measured permeance and thickness. Given that the permeability-selectivity trade-off of self-standing PIM-1 membranes (>20 μm) typically aligns with the 2008 Robeson upper bound [48], this benchmark was included in Fig. 7B for comparison. Notably, several of the TFCs fabricated on GO/PAN in this work exceeded the 2008 upper bound, achieving the highest selectivity values reported for PIM-1 TFCs to date, and surpassing those of previously reported self-standing PIM-1 membranes.

Their permeability, on the other hand, is lower, attributable to the reduced thickness of the PIM-1 layer. As previously discussed and supported by statistical analysis of PIM-1 TFCs reported in literature (Fig. S6), thinner PIM-1 layers exhibit lower permeability due to higher degree of polymer rigidification.

It should be noted that superglassy polymers such as PIM-1, suffer from severe physical aging. Over time, the polymer chains undergo densification as they relax from a non-equilibrium to an equilibrium state, resulting in a substantial decline in membrane permeability [52].

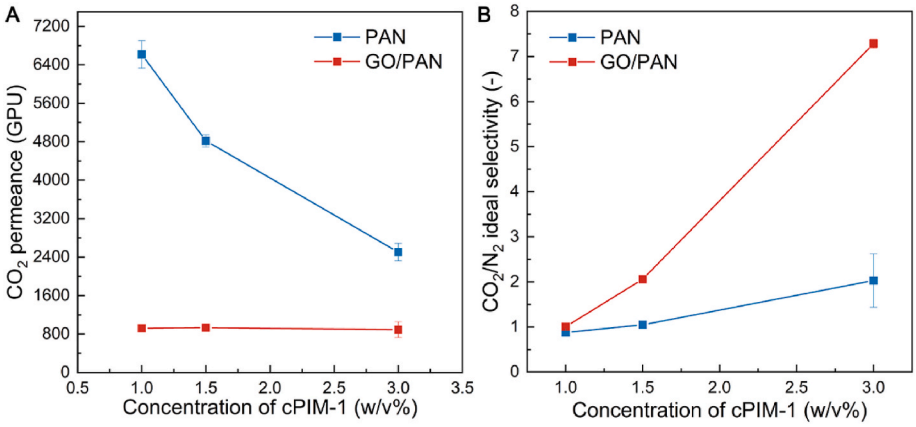

Fig. 8. CO_2 permeance (A) and CO_2/N_2 ideal selectivity (B) of cPIM-1 TFC (GO loading of GO/PAN at 1 mg m^{-2} on PAN#1; permeance and selectivity were calculated as the average value of at least three measurements).

The physical aging behaviour of PIM-1 TFCs fabricated on GO/PAN substrates (GO loading of 1 mg m^{-2} on PAN#2) was evaluated over 110 days (Fig. S7). All membranes exhibited significant reductions in CO_2 permeance, ranging from 75 % to 97 %, which aligns with the reported range for PIM-1 TFCs (50–99 % decline over 100 days). These results suggest that interfacial rigidification induced by GO is insufficient to prevent long-term densification of the polymer matrix. This limitation could be attributed to non-uniform constraints on polymer chain mobility. Therefore, for maintaining the permeance of membranes over longer term, a broader and more uniform interaction, such as a network filler within polymer matrix, could be preferable [22].

To further validate the effectiveness of the GO gutter layer strategy, cPIM-1, another member of the PIMs family, was also investigated. Compared to PIM-1, cPIM-1 solutions exhibit lower viscosity at equivalent concentrations, making them more prone to penetrate into porous PAN substrates during coating [21]. In this context, the use of a GO gutter layer was again found to significantly improve membrane performance.

As shown in Fig. 8, cPIM-1 TFCs coated on bare PAN substrates using solutions ranging from 1 to 3 w/v% (in tetrahydrofuran) exhibited low CO_2/N_2 selectivities (0.9–2.0) and high CO_2 permeances (2505–6615 GPU), primarily due to defect formation caused by polymer penetration. In contrast, when a 1 mg m^{-2} of GO gutter layer was introduced, the ideal CO_2/N_2 selectivity markedly increased. For instance, the selectivity of a cPIM-1 TFC coated with a 3 w/v% solution on GO/PAN increased to 7.3, which is 2.6 times higher than that of its counterpart on bare PAN. Simultaneously, CO_2 permeance dropped to ~822–917 GPU, indicating the suppression of non-selective voids or interfacial defects. The relatively low permeability of cPIM-1 TFC compared to PIM-1 can be mainly attributed to intrinsicly lower fractional free volume in cPIM-1 matrix [38].

4. Conclusions

Here we developed and validated the use of GO as a gutter layer on porous polymeric substrates for the preparation of PIM-1 TFC membranes with enhanced gas separation performance. The optimum GO loading was found to be 1 mg m^{-2}, covering ~47 % of the PAN substrate surface. This partial coverage significantly reduced polymer penetration during membrane fabrication via kiss coating while ensuring robust attachment between the active layer and the PAN. Consequently, the reduced penetration of PIM-1 into the substrate decreased the effective thickness of the active layer and prevented defects that typically occur during coating. With GO as the gutter layer, the ideal CO_2/N_2 selectivity of a fresh PIM-1 TFC improved to up to 44.4, while the CO_2 permeance increased to 3062 GPU, positioning it as the best performing candidate among the state-of-the-art PIM-1 TFCs. Importantly, the strategy was found also effective for active layers of carboxylated cPIM-1. The development of the new strategy can address the common issue of polymer penetration into substrates during TFC membrane fabrication, and hence reduce the increased effective thickness and defects, thereby diminishing the separation performance of TFC membranes. Given the feasibility of this strategy, it holds substantial potential for application across various superglassy polymers, paving the way for making high-performance TFC membranes.

CRediT authorship contribution statement

Boya Qiu: Writing – original draft, Investigation, Formal analysis. **Ming Yu:** Investigation. **Mustafa Alshurafa:** Investigation. **Pablo López-Porfiri:** Writing – review & editing, Investigation. **Maria Perez-Page:** Writing – review & editing, Supervision, Funding acquisition. **Andrew B. Foster:** Writing – review & editing, Resources, Investigation, Formal analysis. **Peter M. Budd:** Writing – review & editing, Supervision, Resources, Funding acquisition. **Xiaolei Fan:** Writing – review & editing, Supervision, Project administration, Funding acquisition. **Patricia Gorgojo:** Writing – review & editing, Supervision, Project administration, Funding acquisition, Conceptualization.

Declaration of competing interest

The authors declare that they have no known competing financial interests or personal relationships that could have appeared to influence the work reported in this paper.

Acknowledgements

P.G. is grateful to the Spanish Ministerio de Economía y Competitividad and the European Social Fund for her Ramon y Cajal Fellowship (RYC2019-027060-I/AEI/10.13039/501100011033). B.Q. thanks to the China Scholarship Council (CSC, file no. 202006240076)-University of Manchester joint studentship for supporting the PhD research. This project has received funding from the European Union's Horizon 2020 research and innovation program under grant agreement No 872102. A.B.F. is supported by EPSRC Programme Grant "SynHiSel" (EP/V047078/1).

Appendix A. Supplementary data

Supplementary data to this article can be found online at https://doi.org/10.1016/j.memsci.2025.124245.

Data availability

Data will be made available on request.

References

[1] R.W. Baker, Gas Separation, Membrane Technology and Applications, 2004, pp. 301–353, https://doi.org/10.1002/0470020393.ch8.

[2] H.B. Park, J. Kamcev, L.M. Robeson, M. Elimelech, B.D. Freeman, Maximizing the right stuff: the trade-off between membrane permeability and selectivity, Science 356 (6343) (2017) eaab0530, https://doi.org/10.1126/science.aab0530.

[3] H.B. Park, C.H. Jung, Y.M. Lee, A.J. Hill, S.J. Pas, S.T. Mudie, E. Van Wagner, B. D. Freeman, D.J. Cookson, Polymers with cavities tuned for fast selective transport of small molecules and ions, Science 318 (5848) (2007) 254–258, https://doi.org/10.1126/science.1146744.

[4] N.B. McKeown, P.M. Budd, Polymers of intrinsic microporosity (PIMs): organic materials for membrane separations, heterogeneous catalysis and hydrogen storage, Chem. Soc. Rev. 35 (8) (2006) 675–683, https://doi.org/10.1039/B600349D.

[5] Y. Wang, B.S. Ghanem, Z. Ali, K. Hazazi, Y. Han, I. Pinnau, Recent progress on polymers of intrinsic microporosity and thermally modified analogue materials for membrane-based fluid separations, Small Struct. 2 (9) (2021) 2100049, https://doi.org/10.1002/sstr.202100049.

[6] R. Swaidan, B. Ghanem, I. Pinnau, Fine-tuned intrinsically ultramicroporous polymers redefine the permeability/selectivity upper bounds of membrane-based air and hydrogen separations, ACS Macro Lett. 4 (9) (2015) 947–951, https://doi.org/10.1021/acsmacrolett.5b00512.

[7] B. Comesaña-Gándara, J. Chen, C.G. Bezzu, M. Carta, I. Rose, M.-C. Ferrari, E. Esposito, A. Fuoco, J.C. Jansen, N.B. McKeown, Redefining the robeson upper bounds for CO2/CH4 and CO2/N2 separations using a series of ultrapermeable benzotriptycene-based polymers of intrinsic microporosity, Energy Environ. Sci. 12 (9) (2019) 2733–2740, https://doi.org/10.1039/C9EE01384A.

[8] G. Genduso, W. Ogieglo, Y. Wang, I. Pinnau, Carbon molecular sieve gas separation materials and membranes: a comprehensive review, J. Membr. Sci. 699 (2024) 122533, https://doi.org/10.1016/j.memsci.2024.122533.

[9] P. Bernardo, E. Drioli, G. Golemme, Membrane gas separation: a review/state of the art, Ind. Eng. Chem. Res. 48 (10) (2009) 4638–4663, https://doi.org/10.1021/ie8019032.

[10] M. O'Keeffe, O.M. Yaghi, Deconstructing the crystal structures of metal–organic frameworks and related materials into their underlying nets, Chem. Rev. 112 (2) (2012) 675–702, https://doi.org/10.1021/cr200205j.

[11] Y.-S. Bae, R.Q. Snurr, Development and evaluation of porous materials for carbon dioxide separation and capture, Angew. Chem. Int. Ed. 50 (49) (2011) 11586–11596, https://doi.org/10.1002/anie.201101891.

[12] Y. Ying, S.B. Peh, H. Yang, Z. Yang, D. Zhao, Ultrathin covalent organic framework membranes via a multi-interfacial engineering strategy for gas separation, Adv. Mater. 34 (25) (2022) 2104946, https://doi.org/10.1002/adma.202104946.

[13] M.M. Khan, V. Filiz, G. Bengtson, S. Shishatskiy, M. Rahman, V. Abetz, Functionalized carbon nanotubes mixed matrix membranes of polymers of intrinsic microporosity for gas separation, Nanoscale Res. Lett. 7 (1) (2012) 504, https://doi.org/10.1186/1556-276X-7-504.

[14] R.S. Bhavsar, T. Mitra, D.J. Adams, A.I. Cooper, P.M. Budd, Ultrahigh-permeance PIM-1 based thin film nanocomposite membranes on PAN supports for CO2 separation, J. Membr. Sci. 564 (2018) 878–886, https://doi.org/10.1016/j.memsci.2018.07.089.

[15] I. Borisov, D. Bakhtin, Jose M. Luque-Alled, A. Rybakova, V. Makarova, A.B. Foster, W.J. Harrison, V. Volkov, V. Polevaya, P. Gorgojo, E. Prestat, P.M. Budd, A. Volkov, Synergistic enhancement of gas selectivity in thin film composite membranes of PIM-1, J. Mater. Chem. A 7 (11) (2019) 6417–6430, https://doi.org/10.1039/C8TA10691F.

[16] E. Aliyev, J. Warfsmann, B. Tokay, S. Shishatskiy, Y.-J. Lee, J. Lillepaerg, N. R. Champness, V. Filiz, Gas transport properties of the metal–organic framework (MOF)-assisted polymer of intrinsic microporosity (PIM-1) thin-film composite membranes, ACS Sustain. Chem. Eng. 9 (2) (2021) 684–694, https://doi.org/10.1021/acssuschemeng.0c06297.

[17] A.B. Foster, J.L. Beal, M. Tamaddondar, J.M. Luque-Alled, B. Robertson, M. Mathias, P. Gorgojo, P.M. Budd, Importance of small loops within PIM-1 topology on gas separation selectivity in thin film composite membranes, J. Mater. Chem. A 9 (38) (2021) 21807–21823, https://doi.org/10.1039/D1TA03712A.

[18] S. Mohsenpour, Z. Guo, F. Almansour, S.M. Holmes, P.M. Budd, P. Gorgojo, Porous silica nanosheets in PIM-1 membranes for CO2 separation, J. Membr. Sci. 661 (2022) 120889, https://doi.org/10.1016/j.memsci.2022.120889.

[19] F. Almansour, M. Alberto, A.B. Foster, S. Mohsenpour, P.M. Budd, P. Gorgojo, Thin film nanocomposite membranes of superglassy PIM-1 and amine-functionalised 2D fillers for gas separation, J. Mater. Chem. A 10 (43) (2022) 23341–23351, https://doi.org/10.1039/D2TA06339E.

[20] B. Zhu, S. He, Y. Yang, S. Li, C.H. Lau, S. Liu, L. Shao, Boosting membrane carbon capture via multifaceted polyphenol-mediated soldering, Nat. Commun. 14 (1) (2023) 1697, https://doi.org/10.1038/s41467-023-37479-9.

[21] M. Yu, A.B. Foster, M. Alshurafa, J.M. Luque-Alled, P. Gorgojo, S.E. Kentish, C. A. Scholes, P.M. Budd, CO2 separation using thin film composite membranes of acid-hydrolyzed PIM-1, J. Membr. Sci. 679 (2023) 121697, https://doi.org/10.1016/j.memsci.2023.121697.

[22] B. Qiu, M. Yu, J.M. Luque-Alled, S. Ding, A.B. Foster, P.M. Budd, X. Fan, P. Gorgojo, High gas permeability in aged superglassy membranes with nanosized UiO-66−NH2/cPIM-1 network fillers, Angew. Chem. Int. Ed. 63 (1) (2024) e202316356, https://doi.org/10.1002/anie.202316356.

[23] Y. Kinoshita, K. Wakimoto, A.H. Gibbons, A.P. Isfahani, H. Kusuda, E. Sivaniah, B. Ghalei, Enhanced PIM-1 membrane gas separation selectivity through efficient dispersion of functionalized POSS fillers, J. Membr. Sci. 539 (2017) 178–186, https://doi.org/10.1016/j.memsci.2017.05.072.

[24] Y. Cheng, X. Wang, C. Jia, Y. Wang, L. Zhai, Q. Wang, D. Zhao, Ultrathin mixed matrix membranes containing two-dimensional metal-organic framework nanosheets for efficient CO2/CH4 separation, J. Membr. Sci. 539 (2017) 213–223, https://doi.org/10.1016/j.memsci.2017.06.011.

[25] B. Ghalei, K. Sakurai, Y. Kinoshita, K. Wakimoto, Ali P. Isfahani, Q. Song, K. Doitomi, S. Furukawa, H. Hirao, H. Kusuda, S. Kitagawa, E. Sivaniah, Enhanced selectivity in mixed matrix membranes for CO2 capture through efficient dispersion of amine-functionalized MOF nanoparticles, Nat. Energy 2 (7) (2017) 17086, https://doi.org/10.1038/nenergy.2017.86.

[26] M. Liu, M.D. Nothling, P.A. Webley, J. Jin, Q. Fu, G.G. Qiao, High-throughput CO2 capture using PIM-1@MOF based thin film composite membranes, Chem. Eng. J. 396 (2020) 125328, https://doi.org/10.1016/j.cej.2020.125328.

[27] R. Hou, S.J.D. Smith, K. Konstas, C.M. Doherty, C.D. Easton, J. Park, H. Yoon, H. Wang, B.D. Freeman, M.R. Hill, Synergistically improved PIM-1 membrane gas separation performance by PAF-1 incorporation and UV irradiation, J. Mater. Chem. A 10 (18) (2022) 10107–10119, https://doi.org/10.1039/D2TA00138A.

[28] Z. Zhou, X. Cao, D. Lv, F. Cheng, Hydrophobic metal–organic framework UiO-66-(CF3)2/PIM-1 mixed-matrix membranes for stable CO2/N2 separation under high humidity, Separ. Purif. Technol. 339 (2024) 126666, https://doi.org/10.1016/j.seppur.2024.126666.

[29] S.K. Elsaidi, M. Ostwal, L. Zhu, A. Sekizkardes, M.H. Mohamed, M. Gipple, J. R. McCutcheon, D. Hopkinson, 3D printed MOF-based mixed matrix thin-film composite membranes, RSC Adv. 11 (41) (2021) 25658–25663, https://doi.org/10.1039/D1RA03124D.

[30] L. Gao, M. Alberto, P. Gorgojo, G. Szekely, P.M. Budd, High-flux PIM-1/PVDF thin film composite membranes for 1-butanol/water pervaporation, J. Membr. Sci. 529 (2017) 207–214, https://doi.org/10.1016/j.memsci.2017.02.008.

[31] M. Alberto, R. Bhavsar, J.M. Luque-Alled, E. Prestat, L. Gao, P.M. Budd, A. Vijayaraghavan, G. Szekely, S.M. Holmes, P. Gorgojo, Study on the formation of thin film nanocomposite (TFN) membranes of polymers of intrinsic microporosity and graphene-like fillers: effect of lateral flake size and chemical functionalization, J. Membr. Sci. 565 (2018) 390–401, https://doi.org/10.1016/j.memsci.2018.08.050.

[32] B. Qiu, M. Alberto, S. Mohsenpour, A.B. Foster, S. Ding, Z. Guo, S. Xu, S.M. Holmes, P.M. Budd, X. Fan, P. Gorgojo, Thin film nanocomposite membranes of PIM-1 and graphene oxide/ZIF-8 nanohybrids for organophilic pervaporation, Separ. Purif. Technol. 299 (2022) 121693, https://doi.org/10.1016/j.seppur.2022.121693.

[33] A.B. Foster, M. Tamaddondar, J.M. Luque-Alled, W.J. Harrison, Z. Li, P. Gorgojo, P. M. Budd, Understanding the topology of the polymer of intrinsic microporosity PIM-1: Cyclics, tadpoles, and network structures and their impact on membrane performance, Macromolecules 53 (2) (2020) 569–583, https://doi.org/10.1021/acs.macromol.9b02185.

[34] J. Contreras-Martínez, S. Mohsenpour, A.W. Ameen, P.M. Budd, C. García-Payo, M. Khayet, P. Gorgojo, High-flux thin film composite PIM-1 membranes for butanol recovery: experimental study and process simulations, ACS Appl. Mater. Interfaces 13 (36) (2021) 42635–42649, https://doi.org/10.1021/acsami.1c09112.

[35] R.R. Nair, H.A. Wu, P.N. Jayaram, I.V. Grigorieva, A.K. Geim, Unimpeded permeation of water through helium-Leak–Tight graphene-based membranes, Science 335 (6067) (2012) 442, https://doi.org/10.1126/science.1211694.

[36] Q. Yang, Y. Su, C. Chi, C.T. Cherian, K. Huang, V.G. Kravets, F.C. Wang, J.C. Zhang, A. Pratt, A.N. Grigorenko, F. Guinea, A.K. Geim, R.R. Nair, Ultrathin graphene-based membrane with precise molecular sieving and ultrafast solvent permeation, Nat. Mater. 16 (12) (2017) 1198–1202, https://doi.org/10.1038/nmat5025.

[37] Y. Han, Z. Xu, C. Gao, Ultrathin graphene nanofiltration membrane for water purification, Adv. Funct. Mater. 23 (29) (2013) 3693–3700, https://doi.org/10.1002/adfm.201202601.

[38] K. Mizrahi Rodriguez, A.X. Wu, Q. Qian, G. Han, S. Lin, F.M. Benedetti, H. Lee, W. S. Chi, C.M. Doherty, Z.P. Smith, Facile and time-efficient carboxylic acid functionalization of PIM-1: effect on molecular packing and gas separation performance, Macromolecules 53 (15) (2020) 6220–6234, https://doi.org/10.1021/acs.macromol.0c00933.

[39] W.S. Hummers, R.E. Offeman, Preparation of graphitic oxide, J. Am. Chem. Soc. 80 (6) (1958) 1339, https://doi.org/10.1021/ja01539a017, 1339.

[40] S. Kwon, K.E. Lee, H. Lee, S.J. Koh, J.-H. Ko, Y.-H. Kim, S.O. Kim, J.Y. Park, The effect of thickness and chemical reduction of graphene oxide on nanoscale friction, J. Phys. Chem. B 122 (2) (2018) 543–547, https://doi.org/10.1021/acs.jpcb.7b04609.

[41] J. Wang, P. Zhang, B. Liang, Y. Liu, T. Xu, L. Wang, B. Cao, K. Pan, Graphene oxide as an effective barrier on a porous nanofibrous membrane for water treatment, ACS Appl. Mater. Interfaces 8 (9) (2016) 6211–6218, https://doi.org/10.1021/acsami.5b12723.

[42] G. Zhao, R. Hu, X. Zhao, Y. He, H. Zhu, High flux nanofiltration membranes prepared with a graphene oxide homo-structure, J. Membr. Sci. 585 (2019) 29–37, https://doi.org/10.1016/j.memsci.2019.05.028.

[43] M. Alberto, R. Bhavsar, J.M. Luque-Alled, A. Vijayaraghavan, P.M. Budd, P. Gorgojo, Impeded physical aging in PIM-1 membranes containing graphene-like fillers, J. Membr. Sci. 563 (2018) 513–520, https://doi.org/10.1016/j.memsci.2018.06.026.

[44] J.M. Luque-Alled, A.W. Ameen, M. Alberto, M. Tamaddondar, A.B. Foster, P. M. Budd, A. Vijayaraghavan, P. Gorgojo, Gas separation performance of MMMs containing (PIM-1)-functionalized GO derivatives, J. Membr. Sci. 623 (2021) 118902, https://doi.org/10.1016/j.memsci.2020.118902.
[45] Z. Liu, Z. Ma, B. Qian, A.Y.H. Chan, X. Wang, Y. Liu, J.H. Xin, A facile and scalable method of fabrication of large-area ultrathin graphene oxide nanofiltration membrane, ACS Nano 15 (9) (2021) 15294–15305, https://doi.org/10.1021/acsnano.1c06155.
[46] R.R. Tiwari, J. Jin, B.D. Freeman, D.R. Paul, Physical aging, CO2 sorption and plasticization in thin films of polymer with intrinsic microporosity (PIM-1), J. Membr. Sci. 537 (2017) 362–371, https://doi.org/10.1016/j.memsci.2017.04.069.
[47] P. Gorgojo, S. Karan, H.C. Wong, M.F. Jimenez-Solomon, J.T. Cabral, A. G. Livingston, Ultrathin polymer films with intrinsic microporosity: anomalous solvent permeation and high flux membranes, Adv. Funct. Mater. 24 (30) (2014) 4729–4737, https://doi.org/10.1002/adfm.201400400.
[48] B. Qiu, Y. Gao, P. Gorgojo, X. Fan, Membranes of polymer of intrinsic microporosity PIM-1 for gas separation: modification strategies and meta-analysis, Nano-Micro Lett. 17 (1) (2025) 114, https://doi.org/10.1007/s40820-024-01610-2.
[49] G. He, S. Huang, L.F. Villalobos, M.T. Vahdat, M.D. Guiver, J. Zhao, W.-C. Lee, M. Mensi, K.V. Agrawal, Synergistic CO2-Sieving from polymer with intrinsic microporosity masking nanoporous single-layer graphene, Adv. Funct. Mater. 30 (39) (2020) 2003979, https://doi.org/10.1002/adfm.202003979.
[50] M. Yu, A.B. Foster, M. Alshurafa, C.A. Scholes, S.E. Kentish, P.M. Budd, Effect of temperature-induced aging on the gas permeation behavior of thin film composite membranes of PIM-1 and carboxylated PIM-1, Ind. Eng. Chem. Res. 63 (37) (2024) 16198–16207, https://doi.org/10.1021/acs.iecr.4c02230.
[51] H.W. Kim, H.W. Yoon, S.-M. Yoon, B.M. Yoo, B.K. Ahn, Y.H. Cho, H.J. Shin, H. Yang, U. Paik, S. Kwon, J.-Y. Choi, H.B. Park, Selective gas transport through few-layered graphene and graphene oxide membranes, Science 342 (6154) (2013) 91, https://doi.org/10.1126/science.1236098.
[52] P.M. Budd, Sieving gases with twisty polymers, Science 375 (6587) (2022) 1354–1355, https://doi.org/10.1126/science.abm5103.